water

MDPI

Article

Vertical Profile Characteristics of Dissolved Organic Matter Biochemistry in the Tropical Reservoir Shaped by Hydrodynamic Forces

Zongyue Liu [1,2,3,4,5,†], Miao Chen [1,2,3,4,5,†], Huiran Liu [2,3,4,5], Han Wang [1,2,3,4,5], Ziyu Ning [1,2,3,4,5], Wen Zhang [1,2,3,4,5], Yuqin Liu [1,2,3,4,5,*] and Min Tang [6,*]

1 College of Ecology, Hainan University, Haikou 570228, China; 22210713000047@hainanu.edu.cn (Z.L.); chenm200567@163.com (M.C.); 2222095132014@hainanu.edu.cn (H.W.); ningziyu18@mails.ucas.ac.cn (Z.N.); wyu58@126.com (W.Z.)
2 Environment and Plant Protection Institute, Chinese Academy of Tropical Agricultural Sciences, Key Laboratory of Low-Carbon Green Agriculture in Tropical Region of China, Ministry of Agriculture and Rural Affairs, Haikou 571101, China; lhr0264@163.com
3 Hainan Danzhou Tropical Agro-Ecosystem National Observation and Research Station, Danzhou 571737, China
4 Hainan Key Laboratory of Tropical Eco-Circular Agriculture, Haikou 571101, China
5 National Agricultural Experimental Station for Agricultural Environment, National Long-Term Experimental Station for Agriculture Green Development, Danzhou 571737, China
6 College of Environmental Science and Engineering, Hainan University, Haikou 570228, China
* Correspondence: liuyq19901106@163.com (Y.L.); tangmin@hainanu.edu.cn (M.T.); Tel./Fax: +86-0898-66969270 (Y.L.)
† These authors contributed equally to this work.

Abstract: Dissolved organic matter (DOM) exerts a crucial role in biogeochemical processes and ascertaining water quality in reservoirs, where it is vulnerable to the dynamic impacts of surface water inflows. However, understanding how DOM quantity and biochemical features responds to hydrodynamic forces in tropical reservoirs remains limited. To enhance our understanding of the vertical profiles of DOM characteristics under varying hydrodynamic forces (strong, moderate, and weak regions) in the Chitian Reservoir (18°43′–18°42′ N, 109°68′–109°70′ E), in December 2023, we investigated the concentrations and biochemical characteristics of water column DOM samples using multispectral techniques, a parallel factor model, and two-dimensional correlation analysis. Our results indicated that DOM concentrations (4.34 ± 0.36 mg/L) are the highest in the reservoir center, whereas total nitrogen (0.52 ± 0.04 mg/L), total phosphorus (0.02 ± 0.03 mg/L), and nitrate nitrogen (1.01 ± 0.07 mg/L) present their highest values in the inlet region. As hydrodynamic force decreases, microbial activity increases, whereas DOM's humification degree and molecular weight decline. DOM in the Chitian Reservoir comprises humic-like components, including three terrestrial sources (accounting for 85.38%~87.03%) and one microbial source, with dominant characteristics of allochthonous origin. The relative abundance of microbial components decreased from 14.62% to 12.97% with the increasing hydrodynamic force and increased with depth. DOM functional groups in the strong hydrodynamic force region and the reservoir's upper layer show high consistency and uniformity. Phenolic O–H is the most reactive functional group concerning changes in water depth across all hydrodynamic areas, followed by polysaccharide C–O, owing to its high photoactivity. In contrast, aromatic C–H demonstrates the weakest reactivity. DOM's spectral features are closely linked to nutrient form concentrations (N and P).

Keywords: hydrodynamic force; tropical reservoir; dissolved organic matter; biochemistry; spatial distribution

check for updates

Academic Editor: Karol Plesiński

Received: 29 November 2024
Revised: 7 January 2025
Accepted: 10 January 2025
Published: 14 January 2025

Citation: Liu, Z.; Chen, M.; Liu, H.; Wang, H.; Ning, Z.; Zhang, W.; Liu, Y.; Tang, M. Vertical Profile Characteristics of Dissolved Organic Matter Biochemistry in the Tropical Reservoir Shaped by Hydrodynamic Forces. *Water* **2025**, *17*, 203. https://doi.org/10.3390/w17020203

Copyright: © 2025 by the authors. Licensee MDPI, Basel, Switzerland. This article is an open access article distributed under the terms and conditions of the Creative Commons Attribution (CC BY) license (https://creativecommons.org/licenses/by/4.0/).

1. Introduction

Dissolved organic matter (DOM) is a complex mixture of organic compounds originating from various sources (for instance, terrestrial or aquatic primary producers) and exhibiting diverse compositions [1,2]. As the most dynamic carbon pool, DOM exerts crucial functions in aquatic element cycling and nutrient exportation, as well as migration and transformation of contaminants [3]. The features of DOM in aquatic environments are impacted not only by the original sources but also the by biogeochemical processes it experiences during transportation [4]. Climate conditions (e.g., temperature, humidity, and precipitation), watershed land use types (e.g., farmland, orchards, natural forests, and grasslands), human activities, hydrological cycles, and biochemical metabolism processes within lakes considerably impact the quantity and quality (e.g., composition, molecular structure, molecular weight) of DOM in these environments, consequently affecting its behavior and fate [5–7]. Comprehending DOM's distribution and biochemical characteristics is of crucial significance for water quality management and the sustainable development of lake ecosystems.

The Chitian Reservoir is located at the intersection of Baoting Li and Miao Autonomous County and Sanya City, covering an area of 220 square kilometers. As a key urban drinking water source for Sanya City, it provides a daily water supply of approximately 250,000 tons, with 89% of the reservoir's water resources originating from upstream Baoting. A combination of allochthonous sources (e.g., domestic wastewater, terrestrial plant residuals, soil erosion, and atmospheric deposition) and autochthonous sources (e.g., the release of algae, phytoplankton, and sediments) influence DOM's components and biochemical characteristics in the Chitian Reservoir [4,8,9]. To the best of our knowledge, most research on DOM in aquatic systems focuses on temperate reservoirs, where the degradation, transformation, and migration processes of DOM exhibit low sensitivity [10]. It is tropical region characterized by high temperatures (33.5 °C) and significant precipitation (1800 mm), experiencing rapid hydrologic cycles. This fast-paced hydrological cycling in the tropical reservoir inevitably change DOM's migration and transform processes, leading to a higher intensity of carbon cycling [11]. The unique climate conditions of Hainan may shape the distinctive characteristics of DOM in tropical reservoirs. However, very few studies focus on the distribution and biochemical characteristics of DOM in tropical reservoirs. Furthermore, previous studies have shown that hydrodynamic conditions can influence water inflow rate, including water retention time. These alterations in retention time can significantly affect the microbial and photocatalytic degradation of DOM in reservoirs [12], leading to variations in DOM distribution, quantity, and composition. For instance, longer retention periods can facilitate the degradation of DOM into smaller-molecular-weight compounds before their downstream transport [6]. What is the vertical distribution of DOM characteristics in the Chitian Reservoir from the entry (strong hydrodynamic force) to the outfall (weak hydrodynamic force)? Evaluating the impact of hydrodynamic forces on DOM's distribution and biochemical features in the tropical reservoir is essential for predicting DOM cycling in the context of increasing anthropogenic and climatic disturbances.

To date, rapid and relatively inexpensive multispectral techniques, such as ultraviolet–visible spectroscopy (UV–vis), excitation–emission matrix (EEM) fluorescence spectroscopy, and Fourier transform infrared (FTIR) spectroscopy, combined with multivariate analyses like parallel factor analysis (PARAFAC), have become essential tools for detecting and characterizing DOM sources, compositions, and molecular structures [13]. Although these techniques provide valuable insights into DOM's sources, biochemical characteristics, and transformations in aquatic environments, the information they yield remains somewhat limited. Two-dimensional correlation spectroscopy (2D-COS) promotes spectral resolution by expanding it into two dimensions [14]. This method also establishes connections

between different probe signals, revealing the sequence of dynamic spectral variations under external perturbations [14–16]. Therefore, 2D-COS analysis of FT-IR spectra offers novel insights into DOM's functional groups' dynamic behavior under hydrodynamic forces. However, this technique in exploring DOM under such external perturbations remains limited. It allows for an in-depth analysis of DOM's response to hydrodynamic forces in both a synchronous and an asynchronous manner.

In this study, water column samples were collected from regions within the Chitian Reservoir characterized by strong (an inlet of an upstream tributary), moderate (center of the reservoir), and weak (reservoir margin) hydrodynamic forces to (1) investigate the vertical and hydrodynamic variations of water physicochemical properties; (2) explore the vertical and hydrodynamic changes of DOM fluorescent signatures using multiple spectroscopic techniques, including UV–vis, 3D-EEMs, FTIR; and (3) elucidate the mechanisms underlying the vertical and hydrodynamic variations of DOM in the reservoir using 2D-COS. This study enhances our understanding of DOM's biogeochemical processes in tropical lake ecosystems and provides theoretical support for their water quality management and sustainable development.

2. Materials and Methods

2.1. Water Sampling

In this study, water samples were collected from three hydrodynamic force regions (denoted as V1, V2, and V3) of the Chitian Reservoir (18°43′–18°42′ N, 109°68′–109°70′ E) in December 2023 (Figure 1). No extreme weather events, such as heavy rainfall, drought, and typhoons, occurred before our sampling period, thus reflecting the typical reservoir conditions of Hainan's tropical region. The strength of the hydrodynamic forces at these sampling sites is as follows: V1 (the tributary entrance of the reservoir, representing the strong hydrodynamic force region) > V2 (the center of the reservoir, representing the moderate hydrodynamic force region) > V3 (the reservoir margin, representing the weak hydrodynamic force region). Three parallel water profiles were sampled in each hydrodynamic force region. A total of 76 water samples were collected across these regions, covering various depths: V1 (1 2, 4, 6, 8, 10, and 12 m), V2 (1, 2, 4, 6, 8, 10, 12, 14, and 16 m), and V3 (1, 2, 4, 6, 8, 10, 12 14, 16, and 18 m). Samples were collected using acid-washed polytetrafluoroethylene bottles and transported to the laboratory within 24 h. Subsequently, one portion of the water was filtered through a 0.45 μm membrane filter and stored at 4 °C for DOM analysis, whereas another portion was used to measure the physicochemical properties. It should be noted that the water samples from the greatest depths contained sediments.

2.2. Physicochemical Parameters Determination

Water sample temperature and pH were measured in situ via a HACH Pocket Pro (USA). The samples were filtered through a 0.45 μm membrane and analyzed directly for dissolved organic carbon (DOC) and total nitrogen (TN) using a multi–N/C 3100 (Analytik Jena, Germany) analyzer. The concentration of ammonia nitrogen (NH_4^+–N) was determined using Nessler's reagent spectrophotometry. The content of total phosphorus (TP) was measured using the ammonium molybdate spectrophotometric method. The nitrate nitrogen (NO_3^-–N) concentrations were measured using colorimetric methods according to Han [17]. The concentration of Fe^{2+} in the water samples was measured photometrically [18].

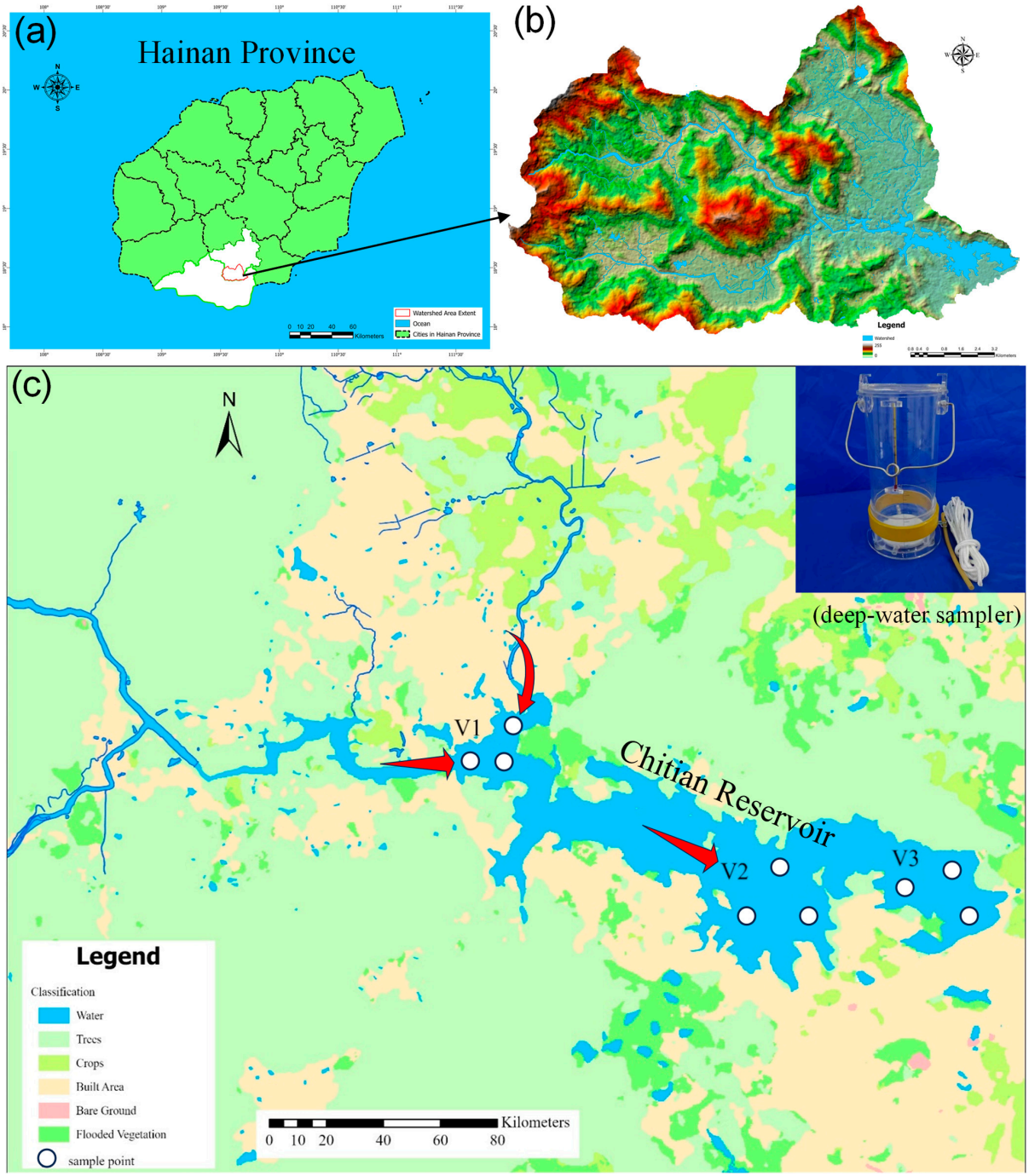


Figure 1. (**a**) Sampling sites location map, (**b**) Sampling sites Digital Elevation Model (DEM) map, (**c**) Distribution of sampling sites in the Chitian Reservoir. V1, V2, and V3 represent the strong, moderate, and weak hydrodynamic force regions, respectively. The red arrow indicates the direction of water flows. Embedded image is water sampler.

2.3. Multiple Spectroscopic Analysis of DOM

DOM samples' UV-vis absorption spectra were obtained using a UV–vis double beam spectrophotometer (UV–2600, Shimadzu, Kyoto, Japan) over the wavelength range of 200–700 nm, with a scanning interval of 1 mm and at medium speed. Ultrapure water served as the blank reference. Four UV–vis optical indices were calculated to assess the chemical properties of DOM: $SUVA_{254}$, spectral slope (S_R), absorption coefficient a_{355}, and absorbance ratio E3/E4. More detailed information about these parameters is shown in Table 1. Fluorescence EEM spectra were obtained using a fluorescence spectrofluorometer (F97 pro,

Lengguang Tech, Shanghai, China) with a scanning speed of 6000 nm·min^{-1}. The scan ranges for emission and excitation were 250–600 nm and 200–500 nm, respectively, corresponding to 5 nm and 1 nm increments. The DOM samples' fluorescent components were obtained based on the PARAFAC analysis of EEM spectra data using the DOMFluor toolbox in MATLAB R2021b [19]. To further characterize the humification and origin of DOM, four fluorescence parameters, including fluorescence index (FI), humification index (HIX), biological index (BIX), and Fn_{355} (estimated from the fluorescence intensity at 300 and 400 nm), were calculated, and more detailed information about these parameters is shown in Table 1. The structure of the DOM compounds was detected via FTIR (Fronter, Perkin Elmerr, Waltham, MA, USA). Specifically, the extracted DOM samples were freeze-dried under vacuum to obtain solid forms. These solids were then combined with KBr of spectral purity in a ratio of 400:1 (*w*/*w*) and pressed into round pellets. The DOM-KBr pellets were scanned with a wavelength range of 400–4000 cm^{-1}. The FT-IR spectral data are processed in OMNIC 8 software.

Table 1. Description of spectral parameters.

Spectral Parameters	Calculation Formula	Symbolic Meaning	References
$SUVA_{254}$	$SUVA_{254}$ = 100× corrected absorbance at 254 nm/DOC concentration	A proxy for the aromaticity of CDOM	[20,21]
S_R	Slope ratio of absorbance at 275–295 nm	A proxy for the molecular weight of CDOM	[21]
E3/E4	E3/E4 = corrected absorbance at 300 nm/corrected absorbance at 400 nm	A proxy for humic origins, E3/E4 > 3.5, DOM is mainly composed of fulvic acid; E3/E4 < 3.5, DOM is mainly composed of humic acid	[22]
a_{355}	a_{355} = 2.303× corrected absorbance at 355 nm/cell path length (0.01 m)	A proxy for the chromophoric DOM (CDOM) content	[23]
FI	FI = F470/F520 at Ex 370 nm, F470/F520 represent the fluorescence intensity at Em wavelength of 470/520 nm	A proxy for fluorescent DOM (FDOM) origins, FI < 1.4 indicate terrestrial origin and FI > 1.8 indicate autochthonous origin	[24]
BIX	BIX = F380/F430 at Ex 310 nm, F380/F430 represent the fluorescence intensity at Em wavelength of 380/430 nm	A proxy for biological activity, BIX > 1 represent abundant freshly produced FDOM	[25]
HIX	HIX = ΣF435–480/ΣF300–345 at Ex 255 nm, ΣF435–480/ΣF300–345 represent the integral fluorescence intensity at Em wavelength of 300–345/435–480 nm	A proxy for humification degree of FDOM	[25]
Fn_{355}	At Ex 355 nm, fluorescence intensity of Em 450	A proxy for the concentration of fluorescent dissolved organic matter	[26]

2.4. 2D-COS Analysis

FT-IR spectra were further analyzed using 2D-COS with the "2DShige 1.3" software to investigate the variation in the functional groups of DOM under different hydrodynamic forces and depths. Detailed procedures for 2D-COS analysis are available in Noda and Ozaki [27].

2.5. Data Analysis

Statistical analyses were carried out in the SPSS Statistics 19.0. Principal component analysis of DOM spectral features and environmental factors was performed using R (version 4.3.3). PARAFAC analysis of EEMs data was conducted in MATLAB. Graphs were generated in Origin 2018.

3. Results and Discussion

3.1. Water Column Physicochemical Properties

The vertical profiles of water properties in the Chitian Reservoir are depicted in Figure 2. The water temperature ranged from 20.6 to 23.4 °C, with the V3 region exhibiting lower temperatures than the V1 and V2 regions. This difference may be attributable to the varying sampling times; V3 water column samples were collected in the morning, while

V1 and V2 samples were collected in the afternoon. However, across all hydrodynamic regions, water temperature consistently decreased with depth. The pH ranged from 6.83 to 7.61, following the V2 > V1 > V3 sequence. In the V1 and V2 regions, pH values increased with depth, while in the V3 region, pH values decreased. The DOC concentration varied within ranges of 2.58–4.36 mg/L at V1, 3.53–8.68 mg/L at V2, and 2.53–3.93 mg/L at V3, respectively, with the overall sequence of V2 > V1 > V3. The highest DOC concentration in the V2 region may be due to its central position within the reservoir, which is subject to hydrodynamic forces from the V1 region (located at the reservoir's runoff inlet) and the littoral water body backflow from the V3 region, resulting in the accumulation of DOC in this area [28], whereas V3, near the dam with the deepest water depth, likely experiences dilution effects, resulting in the lowest DOC content. On the vertical profile, there were no obvious differences in DOC concentration in the overlying water, whereas the bottom layer (the sediment–water interface) exhibited the highest DOC concentration in all regions, indicating the release of sediment. The TP, TN, and NO_3^-–N concentrations were highest in the V1 region, with no significant differences between the V2 and V3 regions. Such high concentrations of TP, TN, and NO_3^-–N in the inlet region (V1) can be attributable to nitrogen and phosphorus inputs from upstream tributaries, which may include sources such as farmland runoff, livestock production, and domestic sewage. This influx also supports the growth of water hyacinths on the surface layer of the V1 region. As the water hyacinth absorbs nutrients, microbial degradation, downward deposition, and physical dilution processes significantly decrease nutrient concentrations in the V2 and V3 regions. Consequently, the TN and NO_3^-–N concentrations exhibited an increasing trend with depth in V1. Meanwhile, the release of bottom sediments may also contribute to this phenomenon. NH_4^+–N and Fe^{2+} concentrations displayed minimal variation across sampling sites and depths; however, their concentrations increased significantly in the bottom samples, reaching values an order of magnitude higher than those observed in other water samples.

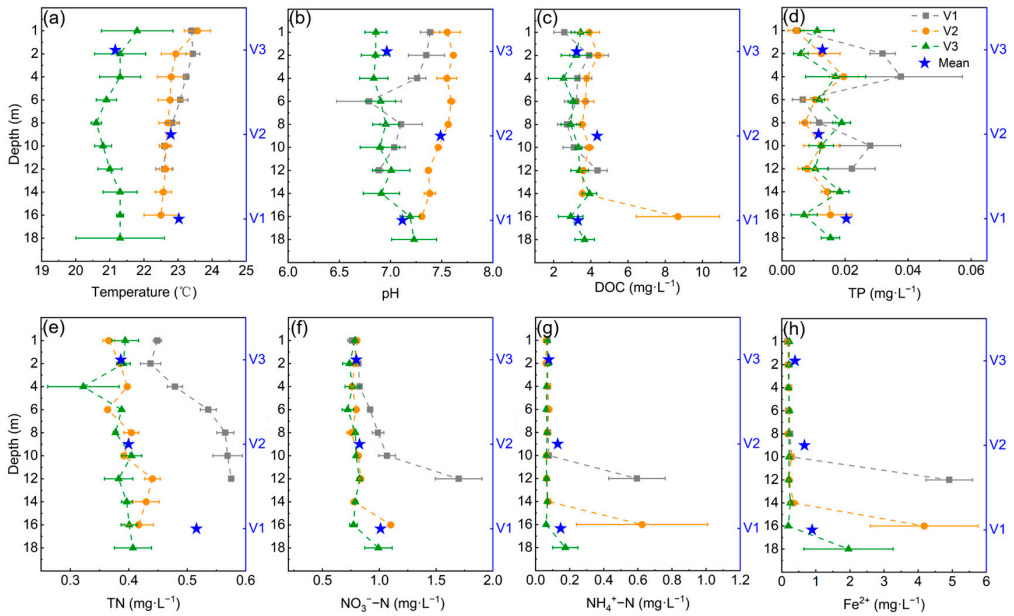


Figure 2. Vertical profiles of temperature (**a**), pH (**b**), DOC (**c**), TP (**d**), TN (**e**), NO_3^-–N (**f**), NH_4^+–N (**g**) and Fe^{2+} (**h**) across different hydrodynamic regions. The "★" symbol indicates the mean value of water column samples under different hydrodynamic forces.

3.2. Spectral Signatures of DOM

Optical indices were analyzed across different hydrodynamic forces and depths (Figure 3) to investigate the source and structure characteristics of DOM in the Chitian Reservoir. The $SUVA_{254}$ index exhibited the highest mean value in V3 (Figure 3a), followed by V1 and V2. This is attributed to the weak hydrodynamic region with a longer water retention time, allowing for sufficient photodegradation and the formation of numerous photo–produced aromatics [29]. These aromatic compounds can enhance the biodegradation of complex substances, thereby contributing to an increase in microbial activity in this area (Figure 3f). This result indicates that the DOM in regions with the weakest hydrodynamic force have the highest aromaticity [30,31]. Notably, the $SUVA_{254}$ value at the bottom layer (i.e., the sediment–water interface) of the reservoir was lower than that of the other layers, which is in line with the findings of Butturini [32]. In the bottom areas, under extreme conditions (perpetual darkness, anoxic, and reduced states), intense microbial activity within organic sediments transforms DOM molecules into saturated, reduced, and non-aromatic compounds [32]. The absorption spectral slope ratio (S_R) shows an inverse relationship with the molecular weight of DOM [21]. The S_R values increased with the decreasing hydrodynamic force (Figure 3b), suggesting episodic input of low-molecular-weight DOM. The E3/E4 ratios of all DOM samples exceeded 3.5, indicating that the fluorescent component of water column DOM in the study area is primarily composed of fulvic acid (Figure 3c) [22]. The a_{355} values are generally positively associated with the concentration of colored DOM [23]. In different hydrodynamic force regions, no obvious differences were observed in the values of a_{355} (Figure 3d). However, the a_{355} values at the bottom were markedly higher than those in the overlying water, suggesting that sediments contribute substantially to the high concentration of CDOM.

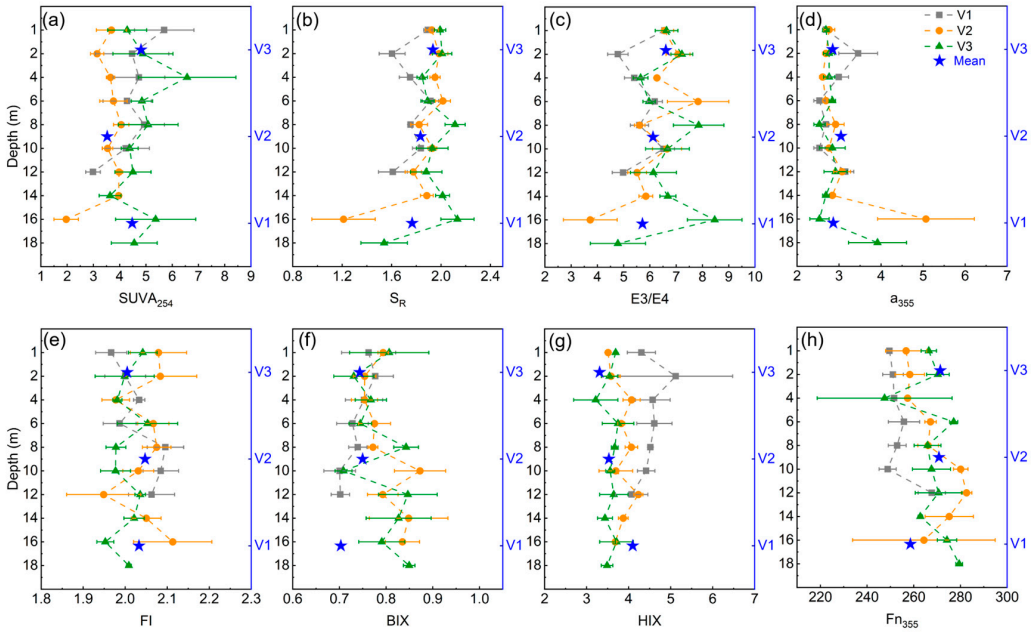


Figure 3. Vertical profiles of DOM spectral indices across different hydrodynamic regions (V1, V2, and V3). $SUVA_{254}$ (**a**), S_R (**b**), E3/E4 (**c**), a_{355} (**d**), FI (**e**), BIX (**f**), HIX (**g**), and Fn_{355} (**h**). The "★" symbol denotes the mean value of water column samples within each different hydrodynamic region.

In all regions, the fluorescence index (FI) ranged from 1.9 to 2.2 (Figure 3e), indicating a high contribution of terrestrial DOM sources [24]. Generally, the biological index (BIX) represents the recently produced DOM from autochthonous and biological sources, whereas the humification index (HIX) indicates DOM's humification degree [25]. As the

hydrodynamic force decreases, BIX values increase following the mean value sequence of V3 > V2 > V1 (Figure 3f). In the vertical profiles, BIX values decrease with depth in the V1 region but increase with depth in the V2 and V3 regions. The increasing BIX values indicate a shift from restricted to active microbial activities [33]. In areas with moderate and weak hydrodynamic forces, intense microbial metabolism reduces the humification degree of DOM. Under vigorous microbial activity, DOM molecules with high humification degrees and complex structures are transformed into smaller molecules [34,35], consistent with the S_R values observed. However, on the vertical profile, the molecular weight (S_R) of water–sediment DOM was significantly higher than that of the overlying water DOM. This is because, at the reservoir bottom, under permanent darkness and anoxic and reduced conditions, microbial metabolism can rapidly transfer low-molecular-weight compounds into large molecular compounds [32]. Consequently, HIX values decrease with the declining hydrodynamic force, following the mean value sequence of V1 > V2 > V3 (Figure 3g). Our samples fall within the HIX value range of 3 to 6, further indicating that terrestrial humified constituents dominated the DOM pool, with relatively fewer biologically derived compounds [36], especially in the inlet region V1. The Fn_{355} values in region V1 are markedly lower than those in regions V2 and V3, suggesting that fluorescent DOM accumulates in areas with weaker hydrodynamic forces (Figure 3h) [26].

3.3. PARAFAC Analysis

PARAFAC analysis successfully decomposed all DOM samples into four fluorescent components (Figure 4a), i.e., humic-like substances originating from different sources (Table 2). Specifically, component 1 (C1), component 2 (C2), and component 3 (C3) are of terrestrial origin, and component 4 (C4) is of microbial origin. As depicted in Figure 4b, the DOM in the Chitian Reservoir, located in a tropical region, comprises humic-like substances without the presence of protein-like substances, including three terrestrial sources (C1, C2, and C3) and one microbial source (C4). This phenomenon aligns with the results obtained by Zhang et al. [37]. The high temperature, intense illumination, and strong microbial metabolism of the Chitian Reservoir in tropical region may contribute to this phenomenon. Yuan et al. [38] suggested that high-temperature reservoir water can enhance the release of humic substances, whereas proteins-like substances are unstable components of DOM, which are easily degraded by microorganisms [28]. The combined percentages of the three terrestrial humic-like components ranged from 85.38% to 87.03% (Figure 4), indicating a predominantly allochthonous sources. As hydrodynamic force decreases, the total percentages of components C1, C2, and C3 decrease from 87.03% to 85.38%. In comparison, the microbial humic-like component (C4) percentage increases from 12.97% to 14.62%, indicating increased microbial activity. This is ascribed to the fact that weaker hydrodynamic regions with longer water retention time facilitate higher microbial metabolism [39]. This trend aligns with the variation observed in the BIX index (Figure 3b). Interestingly, the vertical distribution of these two groups of fluorescent components (terrestrial and microbial source groups) varies across different hydrodynamic force regions. In the strong hydrodynamic force region (V1), the C4 percentage decreases with depth, whereas in the moderate and weak hydrodynamic force regions (V2 and V3), the C4 percentage increases with depth.

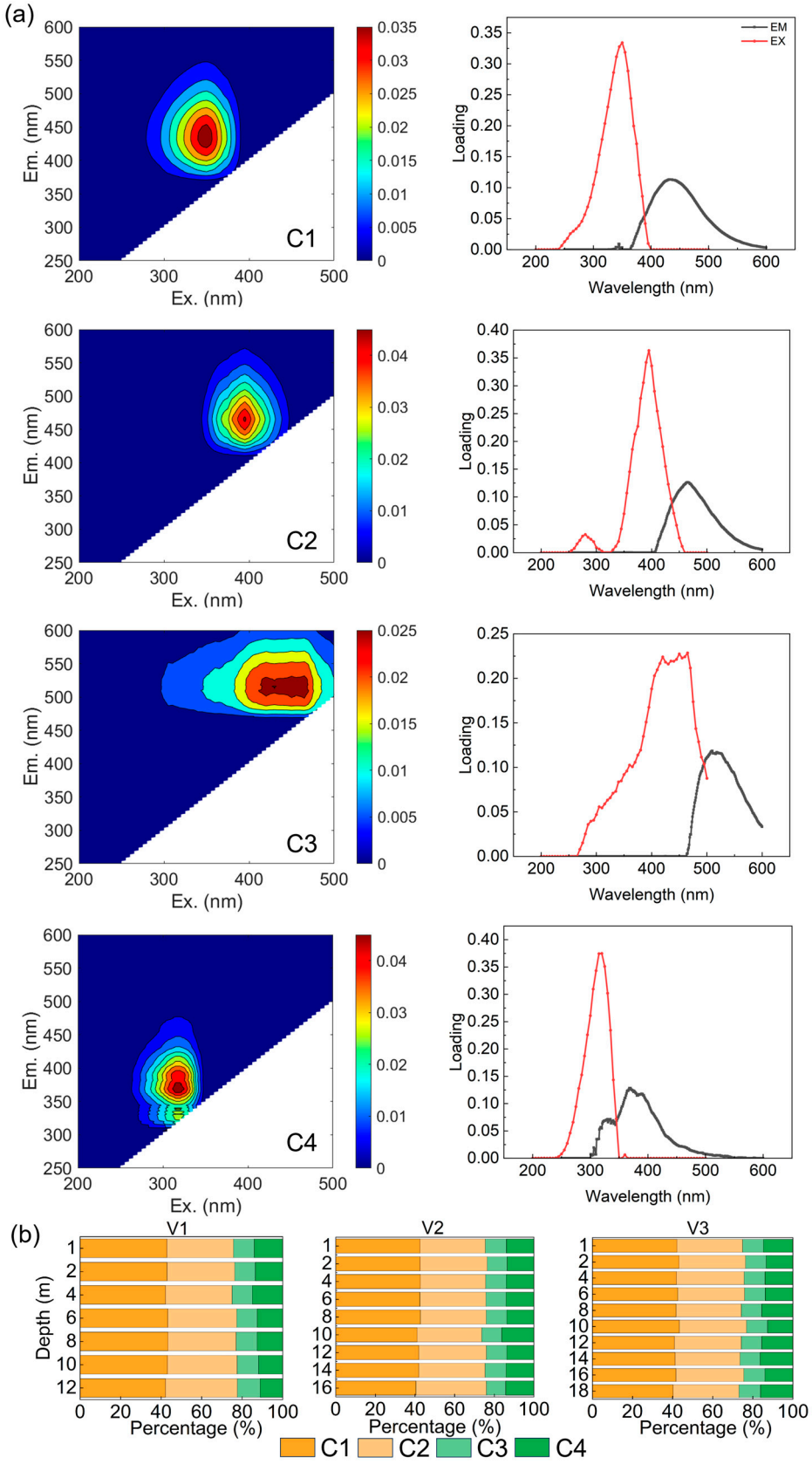


Figure 4. Contour plots (**a**) and relative intensity (**b**) of four fluorescent components in the Chitian Reservoir DOM derived from PARAFAC analysis. V1, V2, and V3 represent regions of strong, moderate, and weak hydrodynamic forces, respectively.

Table 2. PARAFAC components of DOM in the Chitian Reservoir.

Component	Ex (nm)	Em (nm)	Peak Type	References
C1	350	435	Humic-like DOM of terrestrial origin	[40,41]
C2	395	465	Allochthonous humic-like and sensitive to dark	[42,43]
C3	465	510	Traditionally terrestrial humic-like	[44,45]
C4	329	368	Microbial humic-like substances	[46,47]

3.4. Functional Group Variations of DOM

The FT-IR spectra of all water column DOM samples exhibited six major absorption peaks at 3396, 2940, 1630, 1385, 1059, and 865 cm^{-1}, respectively (Figure 5, Table 3), showing varying transmittance under different hydrodynamic forces. The DOM in the Chitian Reservoir mainly is primarily composed of O–H, C–H, and C–O functional groups, originating from phenol, carbohydrate, carboxylic acid, aliphatic, and polysaccharide or polysaccharide-like compounds. Among these, the percentage of the O–H functional group associated with phenol, carbohydrate, and carboxylic acid compounds (at 3396 cm^{-1}) increases as the hydrodynamic force decreases, with percentages of 42.96%, 46.57%, and 47.26% for regions V1, V2, and V3, respectively. This phenomenon was consistent with the results obtained by Fan et al. [48], who showed that O–H comprised the major functional groups of DOM in water. The percentages of C–H in the phenolic hydroxyl or aliphatic groups (at 1385 cm^{-1}) and C–O in polysaccharide or polysaccharide-like substances (at 1059 cm^{-1}) decrease as the hydrodynamic force decreases. In the strong hydrodynamic force region (V1), there are no significant disparities in the intensity percentages of functional groups at different depths. However, in the moderate and weak hydrodynamic force regions (V2 and V3), the intensity percentages of functional groups demonstrate a distinct depth dependency. The percentages of functional groups at 3396 and 1059 cm^{-1} increase with the depth, suggesting an increase in phenol, carbohydrate, carboxylic acid, and polysaccharide or polysaccharide-like compounds. It should be noted that no $COO-$ functional group peak associated with protein-like compounds was found, which is consistent with the PARAFAC results [49].

3.5. Vertical and Hydrodynamic Dynamic Changes of DOM Functional Groups

To further explore the mechanism of functional group variations in DOM under the influence of hydrodynamic forces and depth, 2D-COS analysis was conducted based on the one-dimensional FT-IR spectral data, as shown in Figure 6. The alterations in water layers and hydrodynamics exerts a substantial influence on the DOM functional groups. Figure 6a reveals the dynamic responses of the DOM functional groups to water depth, encompassing the effects of illumination, temperature, oxygen levels, and microbial activity across different hydrodynamic regions. In the synchronous maps, three positive auto-peaks at (1385, 1385 cm^{-1}), (1059, 1059 cm^{-1}), and (3396, 3396 cm^{-1}) were found in all three regions. The intensities of these auto-peaks were higher in regions V2 and V3 than in region V1, suggesting that the DOM functional groups are less sensitive to depth variations under strong hydrodynamic region. Consequently, the intensity order of auto-peaks differs between regions: in V1, the order is 1059 > 3396 > 1385 cm^{-1}; while in V2 and V3, it is 3396 > 1385 > 1059 cm^{-1}. In the strong hydrodynamic force region (V1), the C–O functional group corresponding to polysaccharide or polysaccharide-like substances is most sensitive to depth variation. In contrast, in the moderate and weak hydrodynamic force regions (V2 and V3), the O–H function group, found in phenol, carbohydrate, and carboxylic acid compounds, is the most sensitive to depth variation. Furthermore, a positive cross-peak (1385, 1059 cm^{-1}) was observed in regions V2 and V3, indicating that these functional groups exhibit similar directional changes as water depth increases. However, a negative

cross-peak (1385, 1059 cm^{-1}) in region V1 indicates that these two functional groups exhibit opposite directional changes with increasing water depth.

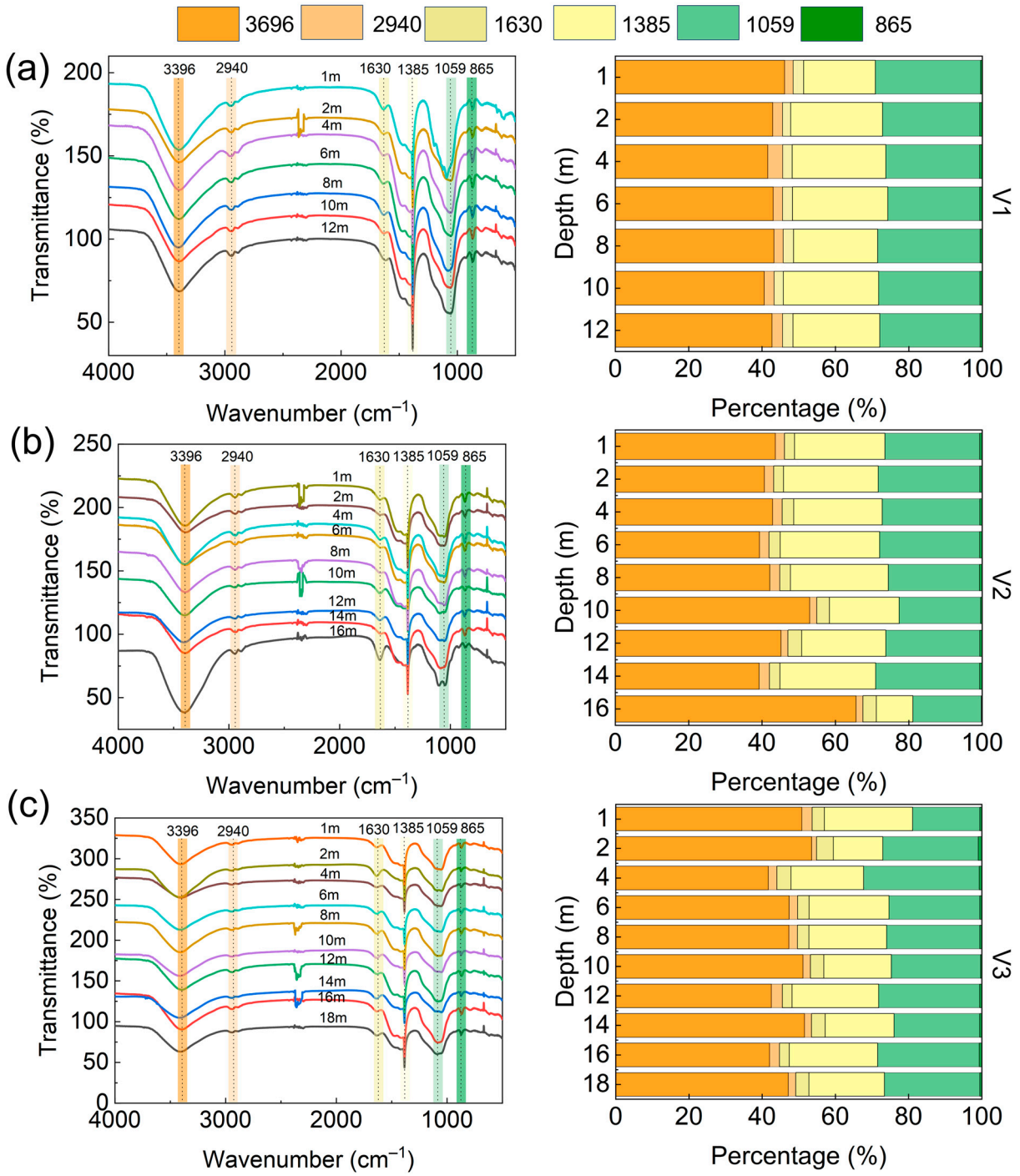


Figure 5. FT-IR spectral characteristics and the relative abundance of high absorption peaks of water column DOM, strong hydrodynamic forces in the V1 region (**a**), moderate hydrodynamic forces in the V2 region (**b**), and weak hydrodynamic forces in the V3 region (**c**).

Table 3. Bands in FT-IR spectra of DOM in the Chitian Reservoir.

Wave Number (cm^{-1})	Functional Group	References
3396	Superimposition of O–H stretching vibrations in phenols, carbohydrates, and carboxylic acids	[50]
2940	C–H stretching vibration within the aliphatic chain	[51]
1630	Stretching of aromatic C=C ring	[49]
1385	Symmetrical bending vibration of C–H in phenolic hydroxylic or aliphatic group	[52]
1059	Stretching vibration of C–O in polysaccharide and polysaccharide-like	[53]
865	Out–of–plane vibrations of aromatic C–H	[54]

In the 2D-FTIR-COS asynchronous spectra (Figure 6a), three positive (1385/1059 cm^{-1}, 3396/1059 cm^{-1}, 3396/2940 cm^{-1}) and two negative (3396/1385 cm^{-1}, 1059/865 cm^{-1}) cross-peaks are observed in the V1 region. In the V2 region, there are three positive (3396/1059 cm^{-1}, 3396/1385 cm^{-1}, 1385/1059 cm^{-1}) and two negative (3396/2904 cm^{-1}, 1059/856 cm^{-1}) cross-peaks. In the V3 region, one positive (1385/1059 cm^{-1}) and two negative (3396/1385 cm^{-1}, 1059/865 cm^{-1}) cross-peaks are detected. According to Noda rules [15], the priority sequence of DOM functional groups is as follows: 1385 → 3396 → 1059 → 2940 → 865 cm^{-1}, 3396 → 1385 → 1059 → 2904 → 865 cm^{-1}, and 1385 → 1059 → 3396 → 865 cm^{-1} for the V1, V2, and V3 regions, respectively, corresponding to the reaction order of phenolic C–H → phenolic O–H → polysaccharide C–O → aliphatic C–H → aromatic C–H, phenolic O–H → phenolic C–H → polysaccharide C–O → aliphatic C–H → aromatic C–H, and phenolic C–H → polysaccharide C–O → phenolic O–H → aromatic C–H.

Figure 6b discloses the dynamic responses of DOM functional groups to hydrodynamic force at the same layers (upper, middle, and bottom). In the synchronous maps, all observed auto-peaks are positive. Among them, two auto-peaks (1059/1059 cm^{-1}, 1385/1385 cm^{-1}) appear in the upper layer; two auto-peaks (3396/3396 cm^{-1}, 1059/1059 cm^{-1}) are found in the middle layer; and two auto-peaks (3396/3396 cm^{-1}, 1385/1385 cm^{-1}) are presented in the bottom layer. The intensities of DOM functional groups increase following the sequence: upper layer < middle layer < bottom layer, indicating increased sensitivity with depth. The C–O functional group, corresponding to polysaccharide or polysaccharide-like substances, shows the highest sensitivity to hydrodynamic force in the upper layer. In contrast, the O–H stretching functional group of phenol, carbohydrate, and carboxylic acid compounds shows the weakest response in the middle and bottom layers. A positive cross-peak (3396/1059 cm^{-1}) is observed in the upper and middle layers, indicating that these two functional groups change in the same direction as hydrodynamic force increases. Conversely, a negative cross-peak (3396/1385 cm^{-1}) in the bottom layer indicates that these two functional groups change in opposite directions as the hydrodynamic conditions vary.

In the asynchronous map of the upper layer, two positive (1059/865 cm^{-1}, 3396/1385 cm^{-1}) and one negative (1385/1059 cm^{-1}) cross-peaks are observed. In the medium layer, two positive (3396/1385 cm^{-1}, 3396/1059 cm^{-1}) and two negative (1059/865 cm^{-1}, 1385/1059 cm^{-1}) cross-peaks are found. In the bottom layer, three positive (3396/2940 cm^{-1}, 1385/1059 cm^{-1}, 1059/865 cm^{-1}) and two negative (3396/1059 cm^{-1}, 3396/1385 cm^{-1}) cross-peaks are exhibited. According to Noda roles [14], the priority sequence of functional groups is as follows: 1059 → 865 → 3396 → 1385 cm^{-1}, 3396 → 1059 → 1385 → 865 cm^{-1}, and 3396 → 2940 → 1385 → 1059 → 865 cm^{-1} for the upper, medium, and bottom layers, respectively, corresponding to the reaction order of polysaccharide C–O → aromatic C–H → phenolic O–H → phenolic C–H, phenolic O–H → polysaccharide C–O → phenolic C–H → aromatic C–H, and phenolic O–H → aliphatic C–H → phenolic C–H → polysaccharide C–O → aromatic C–H.

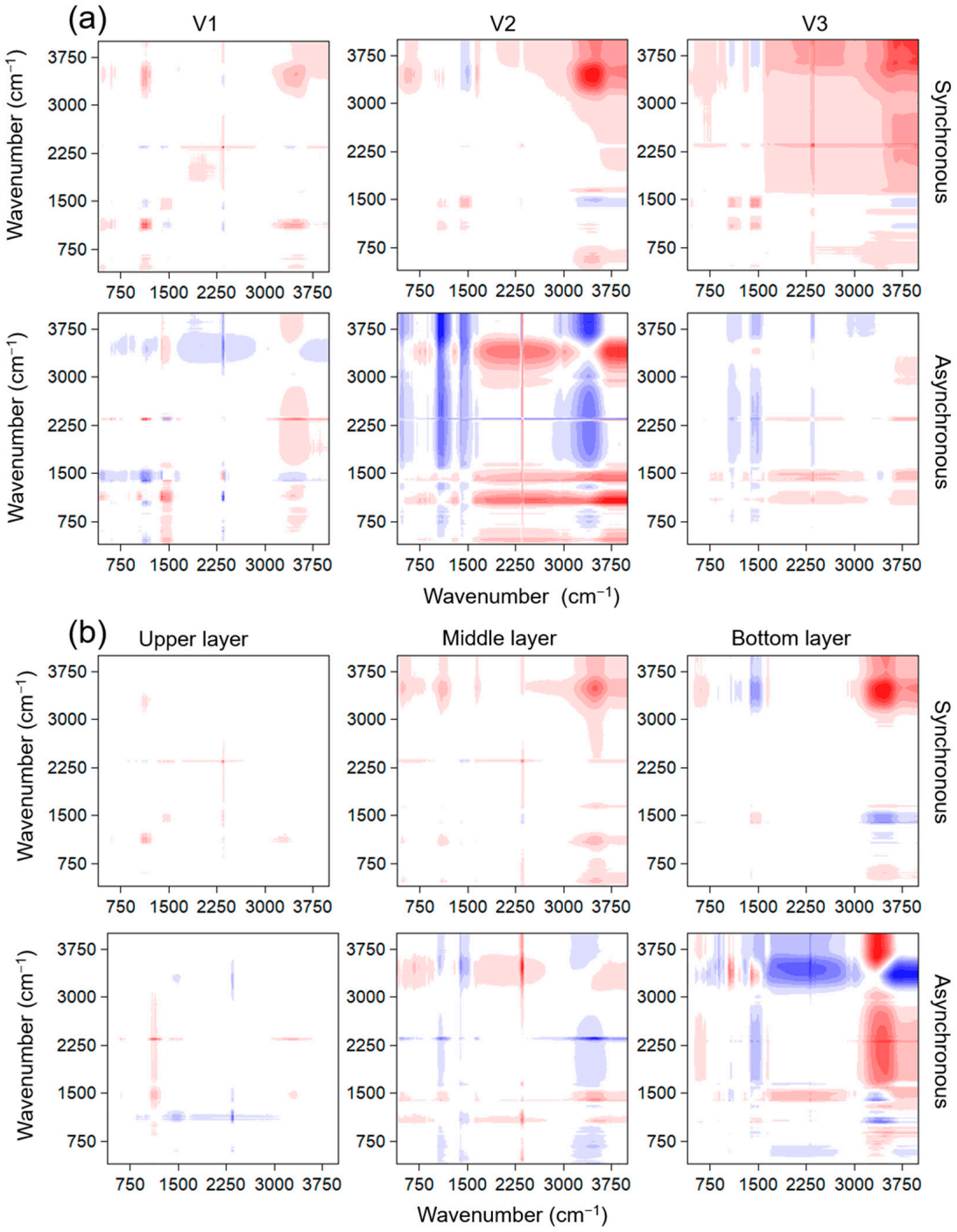


Figure 6. Synchronous and asynchronous maps of water column DOM samples under strong (V1), moderate (V2), and weak (V3) hydrodynamic forces (**a**). Synchronous and asynchronous maps of water DOM samples under different hydrodynamic forces at the same upper, middle, and bottom layers (**b**). In the 2D-COS maps, cross-peaks located in the bottom-right corner were analyzed. Red and blue colors represent the positive and negative correlations, respectively.

According to the above results, we can conclude that both hydrodynamic conditions and depth influence the evolution of DOM functional groups. The DOM functional groups in regions with strong hydrodynamic force and in the upper layer show weak responses to depth and hydrodynamic variations, respectively. This finding suggests that water quality is more uniformly mixed in areas with strong hydrodynamic force and within the upper layer. The phenolic O–H group is the most sensitive and reactive functional group to

depth variation across all regions, followed by the polysaccharide C–O group. The high sensitivity of phenolic O–H is due to the photoactivity of phenolic compounds, which degrade rapidly when exposed to sunlight [55,56]. Polysaccharides, commonly produced by algae, are abundant in natural waters [57]. Polysaccharides are prone to photooxidative degradation under certain conditions, such as the presence of oxygen and light [58]. This result explains why the polysaccharide C–O group exhibits the highest reactivity in the upper layer. In contrast, the aromatic C–H bond shows the lowest reactivity in all regions, which is attributable to its high bond dissociation energy (112.9 kcal·mol^{-1}) [59].

3.6. Correlation Analysis

Pearson correlation analyses between water properties and DOM spectral characteristics under different hydrodynamic forces are presented in Figure 7. Hydrodynamic force significantly influences the vertical profiles of the water's physicochemical properties and the biochemical characteristics of DOM, as indicated by the distinct relationships between parameters under varying hydrodynamic conditions (Figure 7a–c). For instance, depth shows a significant negative correlation with pH in the V1 ($p < 0.05$) and V2 ($p < 0.01$) regions, while it exhibits a significant positive correlation in the V3 region ($p < 0.01$). Overall, there is a positive correlation between depth/DOC concentration and nutrients (TP, TN, NO_3^-–N, and NH_4^+–N) (Figure 7a–c), consistent with the findings of previous studies [60]. This trend may be attributed to sediment release and the constraints of environmental factors at the bottom (e.g., sunlight, temperature, and pH), which reduce microbial nutrient absorption [33]. DOC content shows a positive correlation with NH_4^+–N, suggesting that NH_4^+–N could serve as an indicator of DOM mineralization processes in the context of redox changes [34,61]. DOC content is also positively associated with Fe^{2+} levels across the profiles ($p < 0.01$, Figure 7d,e). This observation implies that DOM may be released from Fe^{3+} oxides during the reduction process ($Fe^{3+} \rightarrow Fe^{2+}$) [25,62]. As expected, the three terrestrial source constituents are positively associated with one another ($p < 0.05$) (Figure 7a–c), whereas the microbial source constituent is positively associated with the BIX index ($p < 0.05$), proving its microbial origin, as verified by the EEM-PARAFAC results (Figure 4). Furthermore, C4 is inversely associated with temperature ($p < 0.05$), and temperature is inversely associated with water depth, indicating that microbial activity increases with water depth. The higher temperature in the upper layer is less conducive to microbial growth, resulting in an increased relative content of C4 with depth (Figure 4b). The $SUVA_{254}$ values exhibit a significantly negative correlation with NO_3^-–N and NH_4^+–N contents ($p < 0.05$) across all sampling sites (Figure 7d). According to Li [63], vigorous primary production processes consume large amounts of nitrogen nutrients to produce DOM. However, the HIX index exhibits a positive correlation with TN and TP contents ($p < 0.01$) (Figure 7d), confirming that humic-like components are effective in fixing nutrients [64,65]. In summary, the spectral features of DOM in the Chitian Reservoir are intimately linked to the contents of nutrient forms (N and P). Therefore, DOM's spectral features could be potentially employed to predict the risk of N and P in the Chitian Reservoir [66].

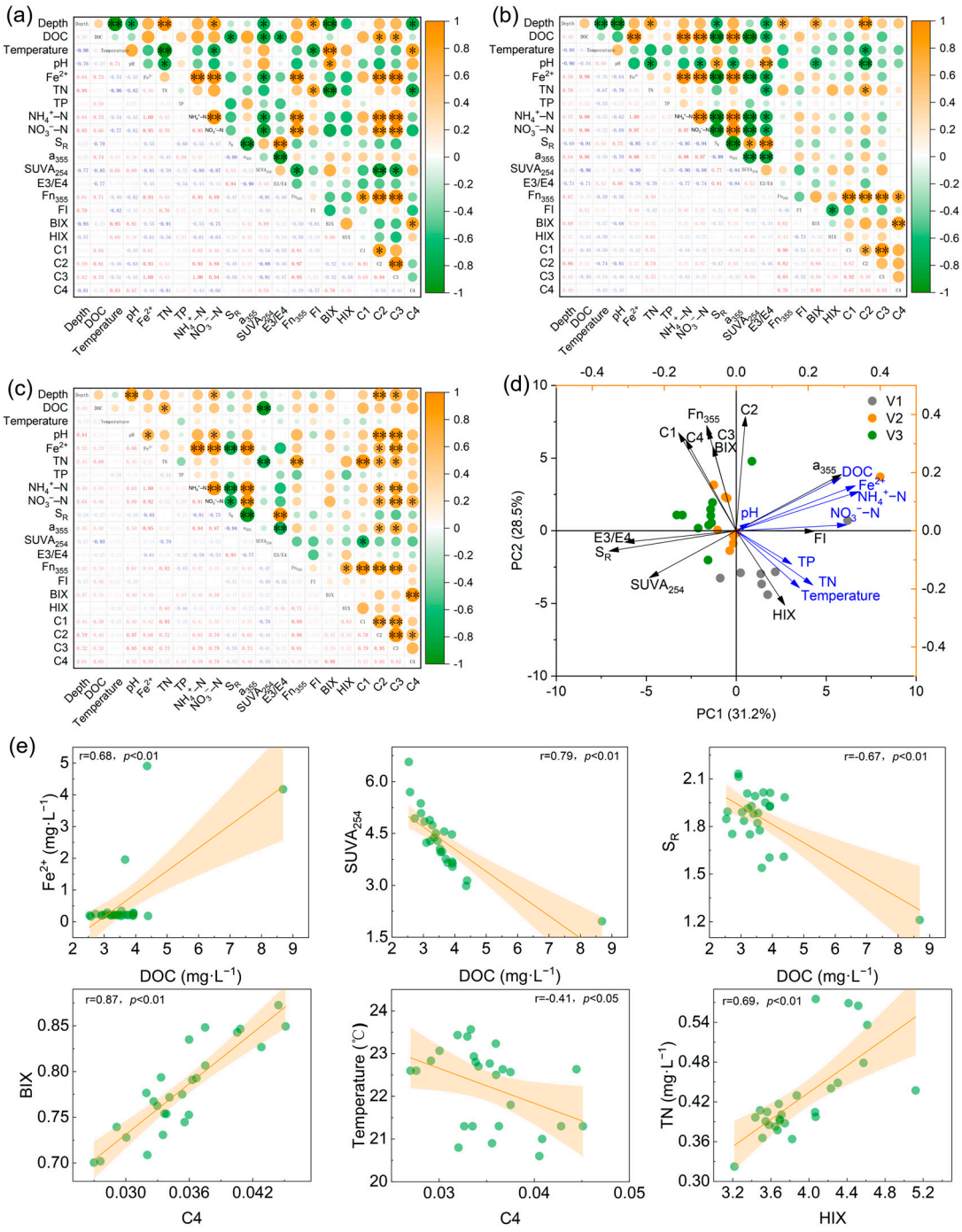


Figure 7. Pearson correlation analysis of water physicochemical parameters and DOM spectral characteristics under strong (**a**), moderate (**b**), and weak (**c**) hydrodynamic forces. Principal component analysis of all water physicochemical and DOM spectral parameters (**d**). Relationships between two parameters (**e**). The orange-shaded area color indicates 95% confidence intervals. * $p \leq 0.05$; ** $p \leq 0.01$. Green dots are samples, Red line is the fitting line.

4. Conclusions

Our study demonstrated that the highest DOC concentrations were in the center of the Chitian Reservoir. The high nutrient levels (TN, TP, and NO_3^-–N) were in the entrance region, potentially indicating a heightened eutrophication risk in this area. In addition, the concentrations of DOC, NO_3^-–N, NH_4^+–N, and Fe^{2+} at the sediment–water interface were considerably higher than those in the overlying water. Spectral analyses suggested that microbial activity increased as hydrodynamic force decreased and depth

increased, leading to a reduction in the humification degree and molecular weight of the DOM in these regions. The DOM in the Chitian Reservoir comprised four humic-like components: three of terrestrial origin and one of microbial origin. Unlike temperate regions, no protein-like components were detected in this tropical reservoir. The distinct climatic conditions of the tropics, characterized by high temperatures, intense illumination, and strong microbial activity, likely account for this difference. The combined percentages of the three terrestrial humic-like components ranged from 85.38% to 87.03%, indicating a dominance of allochthonous sources. The microbial component increased as hydrodynamic force decreased and depth increased. FT-IR spectrum analysis revealed that the major functional groups in the Chitian Reservoir DOM were O–H, C–H, and C–O. The 2D-FT-IR-COS analysis showed that DOM functional groups in the strong hydrodynamic force region and the upper layer exhibited weak responses to depth and hydrodynamic forces due to their high homogeneity. Phenolic O–H was the most reactive functional group to depth variation across all hydrodynamic regions, followed by polysaccharides C–O due to their high photoactivity. However, aromatic C–H showed the weakest reactivity. Correlation analysis confirmed a close link between the spectral features of DOM and nutrient forms (N and P). Consequently, DOM spectral features could be used as indicators to predict the risk of N and P in the Chitian Reservoir.

Author Contributions: Methodology, W.Z.; Software, Z.L., H.W. and Y.L.; Validation, M.T.; Formal analysis, Z.L.; Investigation, Z.L., H.L. and Z.N.; Writing—original draft, Z.L.; Writing—review & editing, M.C. and Y.L.; Supervision, M.C.; Funding acquisition, M.C. and Y.L. All authors have read and agreed to the published version of the manuscript.

Funding: This work was jointly supported by the Chinese Academy of Tropical Agricultural Sciences for the Science and Technology Innovation Team of the National Tropical Agricultural Science Center (No. CATASCXTD202411) and the Central Public-interest Scientific Institution Basal Research Fund for the Chinese Academy of Tropical Agricultural Sciences (No. 1630042023006; 1630042022001).

Data Availability Statement: The raw data supporting the conclusions of this article will be made available by the authors on request.

Conflicts of Interest: The authors declare no conflict of interest.

References

1. Shi, X.; Pereira, R.; Uzma Savege, L.; Poirsat, B.; Quinn, D.; Kostrytsia, A.; Cholet, F.; Smith, C.J.; Gauchotte-Lindsay, C.; Sloan, W.T.; et al. Microbial stratification and DOM removal in drinking water biofilters: Implications for enhanced performance. *Water Res.* **2024**, *262*, 122053. [CrossRef] [PubMed]
2. McDowell, W.H. DOM in the long arc of environmental science: Looking back and thinking ahead. *Biogeochemistry* **2023**, *164*, 15–27. [CrossRef]
3. Lynch, L.M.; Sutfin, N.A.; Fegel, T.S.; Boot, C.M.; Covino, T.P.; Wallenstein, M.D. River channel connectivity shifts metabolite composition and dissolved organic matter chemistry. *Nat. Commun.* **2019**, *10*, 459. Available online: https://www.nature.com/articles/s41467-019-08406-8.pdf (accessed on 28 January 2019). [CrossRef]
4. Wen, Z.D.; Han, J.R.; Shang, Y.X.; Tao, H.; Fang, C.; Lyu, L.L.; Li, S.J.; Hou, J.B.; Liu, G.; Song, K.S. Spatial variations of DOM in a diverse range of lakes across various frozen ground zones in China: Insights into molecular composition. *Water Res.* **2024**, *252*, 121204. [CrossRef]
5. Lin, B.Q.; An, X.Q.; Zhao, C.; Gao, Y.H.; Liu, Y.X.; Qiu, B.; Qi, F.; Sun, D.Z. Analysis of urban composite non-point source pollution characteristics and its contribution to river DOM based on EEMs and FT-ICR MS. *Water Res.* **2024**, *266*, 122406. [CrossRef] [PubMed]
6. Xu, L.; Hu, Q.; Liu, Z.T.; Jian, M.F.; Peng, Y.S.; Shen, R.C.; Liao, W.; Zhong, A.W. Hydrological alteration drives chemistry of dissolved organic matter in the largest freshwater lake of China (Poyang Lake). *Water Res.* **2024**, *251*, 121154. [CrossRef]
7. Abdelrady, A.; Bachwenkizi, J.; Sharma, S.; Sefelnasr, A.; Kennedy, M. The fate of heavy metals during bank filtration: Effect of dissolved organic matter. *J. Water Process Eng.* **2020**, *38*, 101563. [CrossRef]

8. He, J.; Wu, X.; Zhi, G.; Yang, Y.; Wu, L.; Zhang, Y.; Zheng, B.H.; Qadeer, A.; Zheng, J.L.; Deng, W.M.; et al. Fluorescence characteristics of DOM and its influence on water quality of rivers and lakes in the Dianchi Lake basin. *Ecol. Indic.* **2022**, *142*, 109088. [CrossRef]
9. Coble, P.G. Characterization of marine and terrestrial DOM in seawater using excitation-emission matrix spectroscopy. *Mar. Chem.* **1996**, *51*, 325–346. [CrossRef]
10. Wang, K.; Pang, Y.; Gao, C.; Chen, L.; Jiang, X.H.; Li, P.H.; He, C.; Shi, Q.; He, D. Hydrological management affected dissolved organic matter chemistry and organic carbon burial in the Three Gorges Reservoir. *Water Res.* **2021**, *199*, 117195. [CrossRef]
11. Qadafi, M.; Wulan, D.R.; Rosmalina, R.T.; Wulandari, R.; Prayogo, W.; Utami, R.R.; Maulana, Y.E.; Notodarmojo, S.; Zevi, Y. Using UV-Vis differential absorbance spectra of tropical peat water DOM fraction to determine trihalomethanes formation potential and its estimated cytotoxicity. *Water Cycle* **2023**, *4*, 207–215. [CrossRef]
12. Bai, Y.J.; Zhang, S.R.; Mu, E.L.; Zhao, Y.J.; Cheng, L.R.; Zhu, Y.; Yuan, Y.M.; Wang, Y.Y.; Ding, A.Z. Characterizing the spatiotemporal distribution of dissolved organic matter (DOM) in the Yongding River Basin: Insights from flow regulation. *J. Environ. Manag.* **2023**, *325*, 116467. [CrossRef]
13. D'Andrilli, J.; Silverman, V.; Buckley, S.; Rosario-Ortiz, F.L. Inferring ecosystem function from dissolved organic matter optical properties: A critical review. *Environ. Sci. Technol.* **2022**, *56*, 11146–11161. [CrossRef] [PubMed]
14. Noda, I. Generalized two-dimensional correlation spectroscopy. *J. Mol. Spectrosc.* **2004**, *47*, 367–381. [CrossRef]
15. Lin, Z.Y.; Lee, K.H.; Lim, J.Y.; Kim, J.H.; Euu, B.J.; Lee, S.J.; Park, J.Y.; Oh, H.S.; Oh, J. Revealing spatial-temporal impact of industrial effluent towards DOM in Riverine employing PARAFAC and MW-2D COS. *J. Environ. Chem. Eng.* **2024**, *12*, 113412. [CrossRef]
16. Song, F.H.; Li, T.T.; Wu, F.C.; Leung KM, Y.; Hur, J.; Zhou, L.F.; Bai, Y.C.; Zhao, X.L.; He, W.; Ruan, M.Q. Temperature-dependent molecular evolution of biochar-derived dissolved black carbon and its interaction mechanism with polyvinyl chloride microplastics. *Environ. Sci. Technol.* **2023**, *57*, 7285–7297. [CrossRef]
17. Han, Q.; Tong, R.Z.; Sun, W.C.; Zhao, Y.; Yu, J.S.; Wang, G.Q.; Shrestha, S.; Jin, Y.L. Anthropogenic influences on the water quality of the Baiyangdian Lake in North China over the last decade. *Sci. Total Environ.* **2020**, *701*, 134929. [CrossRef]
18. She, Z.X.; Wang, J.; He, C.; Pan, X.; Li, Y.Y.; Zhang, S.Y.; Shi, Q.; Yue, Z.D. The stratified distribution of dissolved organic matter in an AMD lake revealed by multi-sample evaluation procedure. *Environ. Sci. Technol.* **2021**, *55*, 8401–8409. [CrossRef]
19. Stedmon, C.; Rasmus, B. Characterizing dissolved organic matter fluorescence with parallel factor analysis: A tutorial. *Limnol. Oceanogr. -Methods* **2008**, *6*, 572–579. [CrossRef]
20. Li, S.D.; Meng, L.Z.; Zhao, C.; Gu, Y.; Spencer, R.; Salgado, X.A.A.; Kellerman, A.M.; Amy, M.M.; Huang, T.; Yang, H.; et al. Spatiotemporal response of dissolved organic matter diversity to natural and anthropogenic forces along the whole mainstream of the Yangtze River. *Water Res.* **2023**, *234*, 119812. [CrossRef] [PubMed]
21. Helms, J.R.; Stubbins, A.; Ritchie, J.D.; Minor, E.C.; Kieber, D.J.; Mopper, K. Absorption spectral slopes and slope ratios as indicators of molecular weight, source, and photobleaching of chromophoric dissolved organic matter. *Limnol. Oceanogr.* **2008**, *53*, 955–969. [CrossRef]
22. Li, C.Y.; Huang, T.L.; Wen, C.C.; Liang, W.G.; Lin, Z.S.; Yang, S.Y.; Li, K.; Cai, X.C. Influence of storm runoff on the spectral characteristics of dissolved organic matter (DOM) in a drinking water reservoir during the flood season. *Environ. Sci.* **2021**, *42*, 1391–1402. Available online: https://europepmc.org/article/MED/33742936 (accessed on 3 March 2021).
23. Miao, S.; Lyu, H.; Xu, J.; Bi, S.; Guo, H.L.; Mu, M.; Lei, S.H.; Zeng, S.; Liu, H.Q. Characteristics of the chromophoric dissolved organic matter of urban black-odor rivers using fluorescence and UV-visible spectroscopy. *Environ. Pollut.* **2021**, *268*, 115763. [CrossRef] [PubMed]
24. McKnight, D.M.; Boyer, E.W.; Westerhoff, P.K.; Doran, P.T.; Kulbe, T.; Andersen, D.T. Spectrofluorometric characterization of dissolved organic matter for indication of precursor organic material and aromaticity. *Limnol. Oceanogr.* **2001**, *46*, 38–48. Available online: https://aslopubs.onlinelibrary.wiley.com/doi/pdf/10.4319/lo.2001.46.1.0038 (accessed on 18 January 2001). [CrossRef]
25. Chen, M.L.; Kim, S.H.; Jung, H.J.; Hyun, J.H.; Choi, J.H.; Lee, H.J.; Huh, I.A.; Hur, J. Dynamics of dissolved organic matter in riverine sediments affected by weir impoundments: Production, benthic flux, and environmental implications. *Water Res.* **2017**, *121*, 150–161. [CrossRef]
26. Avella, A.R.; Baraër, M.; Mark, B.G.; McKenzie, J.M.; Somers, L. Comparing the performance of three methods to assess DOM dynamics within two distinct glacierized watersheds of the tropical Andes. *Environ. Pollut.* **2020**, *265*, 115052. [CrossRef]
27. Noda, I.; Ozaki, Y. *Two-Dimensional Correlation Spectroscopy-Applications in Vibrational and Optical Spectroscopy*; John Wiley & Sons: Hoboken, NJ, USA, 2005. [CrossRef]
28. Song, F.H.; Wu, F.C.; Feng, W.Y.; Li, S.S.; He, J.; Li, T.T.; Zhang, J.; Wu, A.M.; Dulasiri, A.; Xing, B.S.; et al. Depth-dependent variations of dissolved organic matter composition and humification in a plateau lake using fluorescence spectroscopy. *Chemosphere* **2019**, *225*, 507–516. [CrossRef] [PubMed]

29. Hu, J.; Kang, L.Y.; Li, Z.L.; Feng, X.H.; Liang, C.F.; Wu, Z.; Zhou, W.; Liu, X.N.; Yang, Y.H.; Chen, L.Y. Photo-produced aromatic compounds stimulate microbial degradation of dissolved organic carbon in thermokarst lakes. *Nat. Commun.* **2023**, *14*, 3681. Available online: https://www.nature.com/articles/s41467-023-39432-2.pdf (accessed on 21 June 2023). [CrossRef] [PubMed]
30. Zhu, Y.C.; Jin, Y.; Liu, X.S.; Miao, T.L.; Guan, Q.K.; Yang, R.; Qu, J.J. Insight into interactions of heavy metals with livestock manure compost-derived dissolved organic matter using EEM-PARAFAC and 2D-FTIR-COS analyses. *J. Hazard. Mater.* **2021**, *420*, 126532. [CrossRef]
31. Weishaar, J.L.; Aiken, G.R.; Bergamaschi, B.A.; Fram, M.S.; Fujii, R.; Kenneth, M. Evaluation of specific ultraviolet absorbance as an indicator of the chemical composition and reactivity of dissolved organic carbon. *Environ. Sci. Technol.* **2003**, *37*, 4702–4708. [CrossRef]
32. Burrurini, A.; Herzsprung, P.; Lechtenfeld, O.J.; Venturi, S.; Amalfitano, S.; Vazquez, E.; Pacini, N.; Harper, D.M.; Tassi, F.; Fazi, S. Dissolved organic matter in a tropical saline-alkaline lake of the East African Rift Valley. *Water Res.* **2020**, *173*, 115532. [CrossRef]
33. Ding, H.Y.; Su, J.; Sun, Y.Y.; Yu, H.B.; Zheng, M.X.; Xi, B.D. Insight into spatial variations of DOM fractions and its interactions with microbial communities of shallow groundwater in a mesoscale lowland river watershed. *Water Res.* **2024**, *258*, 121797. [CrossRef] [PubMed]
34. Li, S.D.; Lu, L.F.; Wu, Y.F.; Zhao, Z.L.; Huang, C.C.; Huang, T.; Hao, Y.; Ma, X.H.; Jiang, Q.L. Investigation on depth-dependent properties and benthic effluxes of dissolved organic matter (DOM) in pore water from plateau lake sediments. *Ecol. Indic.* **2021**, *125*, 107500. [CrossRef]
35. Roth, V.N.; Lange, M.; Simon, C.; Hertkorn, N.; Bucher, S.; Goodall, T.; Griffiths, R.I.; Mellado-Vazquez, P.G.; Mommer, L.; Oram, N.J.; et al. Persistence of dissolved organic matter explained by molecular changes during its passage through soil. *Nat. Geosci.* **2019**, *12*, 755–761. [CrossRef]
36. Zhang, Y.L.; Zhang, E.L.; Yin, Y.; van Dijk, M.A.; Feng, L.Q.; Shi, Z.Q.; Liu, M.L.; Qin, B.Q. Characteristics and sources of chromophoric dissolved organic matter in lakes of the Yungui Plateau, China, differing in trophic state and altitude. *Limnol. Oceanogr.* **2010**, *55*, 2645–2659. Available online: https://aslopubs.onlinelibrary.wiley.com/doi/pdf/10.4319/lo.2010.55.6.2645 (accessed on 8 November 2010). [CrossRef]
37. Zhang, L.; Liu, Y.J.; Ge, F.J.; Peng, X.; Li, X.; Zhang, X.Y.; Zhang, S.X.; Zhou, Q.H.; Wu, Z.B.; Liu, B.Y. Spatial characteristics of nitrogen forms in a large degenerating lake: Its relationship with dissolved organic matter and microbial community. *J. Clean. Prod.* **2022**, *371*, 133617. [CrossRef]
38. Yuan, D.N.; Li, S.Y.; Ye CLiu, W.Z.; Xu, J. Dissolved organic matter (DOM) rather than warming and eutrophication directly affects partial pressure of CO_2 (pCO_2) in mesocosm systems. *Water Res.* **2024**, *267*, 122448. [CrossRef] [PubMed]
39. Zhou, L.; Zhou, Y.Q.; Zhang, Y.L.; Wu, Y.H.; Jang, K.S.; Robert, G.M.; Justin, D.B.; Erik, J. Hydrological controls on dissolved organic matter composition throughout the aquatic continuum of the watershed of selin co, the Largest Lake on the Tibetan Plateau. *Environ. Sci. Technol.* **2023**, *57*, 4668–4678. [CrossRef]
40. Murphy, K.R.; Hambly, A.C.; Singh, S.; Henderson, R.K.; Baker, A.; Stuetz, R.; Khan, S.T. Organic matter fluorescence in municipal water recycling schemes: Toward a unified PARAFAC model. *Environ. Sci. Technol.* **2011**, *45*, 2909–2916. [CrossRef]
41. Shutova, Y.; Baker, A.; Bridgeman, J.; Henderson, R.K. Spectroscopic characterisation of dissolved organic matter changes in drinking water treatment: From PARAFAC analysis to online monitoring wavelengths. *Water Res.* **2014**, *54*, 159–169. [CrossRef] [PubMed]
42. Ren, W.X.; Wu, X.D.; Ge, X.G.; Lin, G.Y.; Zhou, M.D.; Long, Z.J.; Yu, X.H.; Tian, W. Characteristics of dissolved organic matter in lakes with different eutrophic levels in southeastern Hubei Province, China. *J. Oceanol. Limnol.* **2021**, *39*, 1256–1276. [CrossRef]
43. Lee, S.A.; Kim, T.H.; Kim, G.B. Tracing terrestrial versus marine sources of dissolved organic carbon in a coastal bay using stable carbon isotopes. *Biogeosciences* **2022**, *17*, 135–144. [CrossRef]
44. Stedmon, C.A.; Markager, S. Tracing the production and degradation of autochthonous fractions of dissolved organic matter by fluorescence analysis. *Limnol. Oceanogr.* **2005**, *50*, 1415–1426. [CrossRef]
45. Liu, C.; Shen, Q.S.; Gu, X.H.; Zhang, L.; Han, C.; Wang, Z.D. Burial or mineralization: Origins and fates of organic matter in the water–suspended particulate matter–sediment of macrophyte– and algae–dominated areas in Lake Taihu. *Water Res.* **2023**, *243*, 120144. [CrossRef] [PubMed]
46. Cory, R.M.; McKnight, D.M. Fluorescence spectroscopy reveals ubiquitous presence of oxidized and reduced quinones in dissolved organic matter. *Environ. Sci. Technol.* **2005**, *39*, 8142–8149. [CrossRef] [PubMed]
47. Hong, H.L.; Wu, S.J.; Wang, Q.; Dai, M.Y.; Lu, Q.; Zhu, H.; Li, J.W.; Zhang, J.; Liu, J.C.; Li, J.; et al. Fluorescent dissolved organic matter facilitates the phytoavailability of copper in the coastal wetlands influenced by artificial topography. *Sci. Total Environ.* **2021**, *790*, 147855. [CrossRef] [PubMed]
48. Fan, T.T.; Yao, X.; Sang, D.L.; Liu, L.; Sun, Z.L.; Deng, H.G.; Zhang, Y.H.; Sun, X. Composition characteristics and metal binding behavior of macrophyte–derived DOM (MDOM) under microbial combined photodegradation: A state closer to actual macrophytic lakes. *J. Hazard. Mater.* **2024**, *465*, 133124. [CrossRef]
49. Liu, S.S.; Feng, W.Y.; Song, F.H.; Li, T.T.; Guo, W.J.; Wang, B.B.; Wang, H.Y.; Wu, F.C. Photodegradation of algae and macrophyte–derived dissolved organic matter: A multi–method assessment of DOM transformation. *Limnologica* **2019**, *77*, 125683. [CrossRef]

50. Chen, B.F.; Huang, W.; Ma, S.Z.; Feng, M.H.; Liu, C.; Gu, X.Z.; Chen, K.N. Characterization of chromophoric dissolved organic matter in the littoral zones of eutrophic lakes Taihu and Hongze during the algal bloom season. *Water* **2018**, *10*, 861. Available online: https://www.mdpi.com/2073-4441/10/7/861 (accessed on 20 June 2018). [CrossRef]
51. Abdulla, H.; Minor, E.C.; Dias, R.F.; Hatcher, P.G. Changes in the compound classes of dissolved organic matter along an estuarine transect: A study using FTIR and 13C NMR. *Geochim. Cosmochim. Acta* **2010**, *74*, 3815–3838. [CrossRef]
52. Ifon, B.E.; Kiki, C.; Lasisi, K.H.; Suanon, F.; Adyari, B.; Wotto, V.; Yu, C.P.; Hu, A.Y. Effects of bisphenols and perfluoroalkylated substances on fluorescence properties of humic and amino acids substances of dissolved organic matter: EEM-PARAFAC and ATR-FTIR analysis. *J. Environ. Chem. Eng.* **2022**, *10*, 108186. [CrossRef]
53. Liu, S.S.; Zhu, Y.R.; Liu, L.Z.; He, Z.Q.; Giesy, J.P.; Bai, Y.C.; Sun, F.H.; Wu, F.C. Cation–induced coagulation of aquatic plant–derived dissolved organic matter: Investigation by EEM–PARAFAC and FT–IR spectroscopy. *Environ. Pollut.* **2018**, *234*, 726–734. [CrossRef]
54. Ji, H.K.; Wang, H.; Wu, Z.P.; Wang, D.F.; Wang, X.L.; Fu, P.J.; Li, C.S.; Deng, W.G. Source, composition and molecular diversity of dissolved and particulate organic matter varied with riparian land use in tropical coastal headstreams. *Sci. Total Environ.* **2024**, *908*, 168577. [CrossRef] [PubMed]
55. Jiang, T.; Kaal, J.; Liang, J.P.; Zhang, Y.L.; Wei, S.Q.; Wang, D.Y.; Green, N.W. Composition of dissolved organic matter (DOM) from periodically submerged soils in the Three Gorges Reservoir areas as determined by elemental and optical analysis, infrared spectroscopy, pyrolysis–GC–MS and thermally assisted hydrolysis and methylation. *Sci. Total Environ.* **2017**, *603*, 461–471. [CrossRef] [PubMed]
56. He, D.; Wang, K.; Pang, Y.; He, C.; Li, P.H.; Li, Y.Y.; Xiao, S.B.; Shi, Q.; Sun, Y.G. Hydrological management constraints on the chemistry of dissolved organic matter in the Three Gorges Reservoir. *Water Res.* **2020**, *187*, 116413. [CrossRef] [PubMed]
57. Stubbins, A.; Dittmar, T. Illuminating the deep: Molecular signatures of photochemical alteration of dissolved organic matter from North Atlantic Deep Water. *Mar. Chem.* **2015**, *177*, 318–324. [CrossRef]
58. Junaid, M.; Wang, J. Interaction of nanoplastics with extracellular polymeric substances (EPS) in the aquatic environment: A special reference to eco–corona formation and associated impacts. *Water Res.* **2021**, *201*, 117319. [CrossRef]
59. Razack, S.A.; Lee, Y.; Bose, S.; Shin, H.; Jung, W.; Kang, H.W. Photo–triggered caffeic acid delivery via psyllium polysaccharide– gellan gum–based injected bionanogel for epidermoid carcinoma treatment. *Int. J. Biol. Macromol.* **2024**, *267*, 131166. [CrossRef] [PubMed]
60. Cheng, L.; Wang, H.H.; Cai, H.R.; Zhang, J.; Gong, X.; Han, W. Iron–catalyzed arene C–H hydroxylation. *Science* **2021**, *374*, 77–81. [CrossRef]
61. Yang, X.M.; Yuan, J.; Yue, F.J.; Li, S.L.; Wang, B.L.; Mohinuzzaman, M.; Liu, Y.J.; Senesi, N.; Lao, X.Y.; Li, L.L.; et al. New insights into mechanisms of sunlight–and dark–mediated high–temperature accelerated diurnal production–degradation of fluorescent DOM in lake waters. *Sci. Total Environ.* **2021**, *15*, 143377. [CrossRef]
62. Frazier, B.E.; Naimo, T.J.; Sandheinrich, M.B. Temporal and vertical distribution of total ammonia nitrogen and un–ionized ammonia nitrogen in sediment pore water from the upper Mississippi River. *Environ. Toxicol. Chem.* **2010**, *15*, 92–99. [CrossRef]
63. Li, X.J.; La, L.M.; Peng, L.; Qiu, L.Q.; Luigi, N.F. Iron operates as an important factor promoting year–round diazotrophic cyanobacteria blooms in eutrophic reservoirs in the tropics. *Ecol. Indic.* **2021**, *125*, 107446. [CrossRef]
64. Li, L.; Zhou, L.; Meng, T.Z.; Yang, Y.; Wang, J.S.; Ren, Q.Q.; Dai, Q.Y. Absorbance and fluorescence spectrums of chromophoric dissolved organic matter in the reed wetland of liaohe estuary. *Peridical Ocean. Univ. China* **2017**, *47*, 27–36. [CrossRef]
65. Newman, S.; Reddy, K.R. Alkaline phosphatase activity in the sediment–water column of a hypereutrophic lake. *J. Environ. Qual.* **1993**, *22*, 832–838. [CrossRef]
66. Dong, Y.; Li, Y.; Kong, F.; Zhang, J.; Xi, M. Source, structural characteristics and ecological indication of dissolved organic matter extracted from sediments in the primary tributaries of the Dagu River. *Ecol. Indic.* **2020**, *109*, 105776. [CrossRef]

Disclaimer/Publisher's Note: The statements, opinions and data contained in all publications are solely those of the individual author(s) and contributor(s) and not of MDPI and/or the editor(s). MDPI and/or the editor(s) disclaim responsibility for any injury to people or property resulting from any ideas, methods, instructions or products referred to in the content.